RESEARCH ARTICLE

Endothelial Surface Glycocalyx Can Regulate Flow-Induced Nitric Oxide Production in Microvessels *In Vivo*

Wanyi Yen, Bin Cai, Jinlin Yang, Lin Zhang, Min Zeng, John M. Tarbell, Bingmei M. Fu*

Department of Biomedical Engineering, The City College of the City University of New York, New York, New York, United States of America

* fu@ccny.cuny.edu

Abstract

Due to its unique location, the endothelial surface glycocalyx (ESG) at the luminal side of the microvessel wall may serve as a mechano-sensor and transducer of blood flow and thus regulate endothelial functions. To examine this role of the ESG, we used fluorescence microscopy to measure nitric oxide (NO) production in post-capillary venules and arterioles of rat mesentery under reduced (low) and normal (high) flow conditions, with and without enzyme pretreatment to remove heparan sulfate (HS) of the ESG and in the presence of an endothelial nitric oxide synthase (eNOS) inhibitor, N^G-monomethyl-L-arginine (L-NMMA). Rats (SD, 250–300g) were anesthetized. The mesentery was gently taken out from the abdominal cavity and arranged on the surface of a glass coverslip for the measurement. An individual post-capillary venule or arteriole was cannulated and loaded for 45 min with 5 μM 4, 5-Diaminofluorescein diacetate, a membrane permeable fluorescent indictor for NO, then the NO production was measured for ~10 min under a low flow (~300 μm/s) and for ~60 min under a high flow (~1000 μm/s). In the 15 min after switching to the high flow, DAF-2-NO fluorescence intensity increased to 1.27-fold of its baseline, DAF-2-NO continuously increased under the high flow, to 1.53-fold of its baseline in 60 min. Inhibition of eNOS by 1 mM L-NMMA attenuated the flow-induced NO production to 1.13-fold in 15 min and 1.30-fold of its baseline in 60 min, respectively. In contrast, no significant increase in NO production was observed after switching to the high flow for 60 min when 1 h pretreatment with 50 mU/mL heparanase III to degrade the ESG was applied. Similar NO production was observed in arterioles under low and high flows and under eNOS inhibition. Our results suggest that ESG participates in endothelial cell mechanosensing and transduction through its heparan sulfate to activate eNOS.

Introduction

The inner surface of blood vessels is lined with endothelial cells coated with a thin layer of endothelial surface glycocalyx (ESG). The ESG consists of proteoglycans, glycosaminoglycans

(GAGs) and glycoproteins [1,2,3,4]. The GAGs in the ESG are heparan sulfate (HS), hyaluronic acid (HA), chondroitin sulfate (CS) and sialic acid (SA), of which, the most abundant one is HS, accounting for 50–90% of the GAGs [2]. Previous studies have shown that the ESG plays an important role in maintaining vessel wall permeability [5,6,7,8] and modulating circulating blood cell-vessel wall interaction [1,9,10,11,12]. Damage of ESG was found in many cardiovascular diseases, diabetes, ischemia/reperfusion, chronic infectious diseases, chronic kidney diseases [3,13,14,15,16] as well as in tumor metastasis [17]. Due to its unique location, the ESG of the microvessel wall may serve as a mechano-sensor and transducer of blood flow.

Nitric oxide (NO), the smallest signaling molecule known [18], is one of the most important protective molecules in the vasculature. Endothelial nitric oxide synthase (eNOS) is responsible for most of the vascular NO production [19,20]. NO regulates vascular tone and blood flow, inhibits platelet aggregation and adhesion, controls vascular smooth muscle proliferation and inhibits leukocyte adhesion and vascular inflammation [18,21,22]. Shear stress generated by blood flow has been demonstrated to induce NO production in coronary vasculature in dogs [23], in various sized arteries (1–8 mm diameter) of pigs [24], in small arteries of rabbits [25] and in a variety of cultured endothelial cells (ECs) [21,26,27,28]. An extensive in silico model that captures the major mechanisms of NO production in endothelial cells has been reported recently [29].

So far, at least ten candidates have been identified as mechano-sensors and transducers, including cell adhesion proteins (e.g., VE-cadherin, PECAM-1) [30,31], ion channels [32,33], tyrosine kinase receptors (e.g. vascular endothelial growth factor receptor 2) [31]; G-protein-coupled receptors and G-proteins [34], caveolae [35], primary cilia [36], actin filaments [37], nesprins [38], and integrins [39]. These structures and molecules of ECs can sense blood flow-induced mechanical stimuli and transmit them into the EC cytoplasm and nucleus to regulate vascular functions. Being the most apical structure of the ECs along with cilia facing the blood flow, the ESG may also serve as a mechanosensor and transducer for the blood flow. Florian et al. [21] found that shear induced NO production was impaired in bovine aortic endothelial cells (BAECs) when heparinase III was used to degrade HS in ESG. Depletion of HS and HA but not CS on BAECs blocks the shear-induced NO production [27]; depletion of HS, HA and CS also inhibits the shear-induced increase in hydraulic conductivity of BAEC monolayers [28]. Degradation of HS inhibits the shear-induced NO production in cultured rat aortic smooth muscle cells [40] and degradation of HA but not CS attenuates the flow-induced NO production in myotubes [41]. Mochizuki and coworkers [42] found that after hyaluronidase treatment, the shear stress-induced NO production was reduced in isolated canine femoral arteries. In an ex vivo study using porcine superficial femoral arteries, Kumagai et al [43] confirmed the role of HA in shear stress-mediated NO mechanotransduction but not HS and SA. Instead, their study implied a role of HS and SA in ROS (reactive oxygen species) regulation in the vessel wall under the shear stress stimulation. Other recent studies have shown that shear stress can alter the distribution of ESG components on the cell surface and their rates of synthesis [29] [44] [45] [46,47].

Although the ESG has been shown to regulate flow-induced NO production in arteries and in cultured arterial ECs, and Van Teeffelen et al [48] indirectly showed that heparin-impaired glycocalyx attenuates shear dependent vasodilation in arterioles of mouse cremaster muscle, there has been no direct study showing that ESG can regulate flow-induced NO production in individual microvessels. Therefore, the objective of this study was to test the hypothesis that the ESG plays a role in mechanosensing and transduction of the microvessel wall through regulating flow-induced NO production. We used fluorescence microscopy and a fluorescent NO indicator, 4, 5-Diaminofluorescein diacetate (DAF-2 DA) to measure the EC NO production [49] in individually cannulated post-capillary venules of rat mesentery under reduced (low)

and normal (high) flow conditions. We have shown recently that these vessels have a substantial ESG characterized by a ~ 1 µm thick HS layer [50]. To examine the role of ESG in NO production, we used heparinase III to selectively degrade the HS of the ESG at the microvessel wall before the NO measurement under the low and high flow conditions. To further investigate the molecular mechanism by which ESG regulates the flow-induced NO production, we measured NO production in the presence of the endothelial nitric oxide synthase (eNOS) inhibitor, N^G-monomethyl-L-arginine (L-NMMA). The results showed that heparinase treatment completely inhibited flow-induced NO production in post-capillary venules.

Materials and Methods

Ethics Statement

All experiments were performed on adult female Sprague–Dawley rats (250–300g), supplied by Hilltop Laboratory Animals (Scottdale, PA). All animal care and preparation procedures were approved by the Animal Care and Use Committee at the City College of the City University of New York (The protocol number is 0899).

Animal Preparation

The methods used to prepare rat mesenteries, perfusion solutions and micropipettes for microperfusion experiments have been described in detail in [17,51,52]. A brief outline of the methods is given below with emphasis on the special features of the current experiments. At the end of experiments the animals were euthanized with excess anesthetic. The thorax was opened to ensure death.

Rats were anesthetized with pentobarbital sodium given subcutaneously at the initial dosage of 65 mg/kg followed by an additional 3 mg/dose when needed. Then the rat was transferred to a tray and kept warm at 37°C on a heating pad and monitored by a thermometer. A mid-line surgical incision (2–3 cm) was made in the abdominal wall. The mesentery was carefully taken out from the abdominal cavity and arranged on a glass coverslip to maintain circulation to the intestine and mesentery. During the entire experiment, the upper surface of the tissue was continuously superfused by a dripper with mammalian Ringer solution at ~37 °C, which was regulated by a controlled water bath and monitored by a thermometer probe. Most microvessels chosen for the study were straight non-branched post-capillary venules, with diameters of ~25–45 µm. Another group contained arterioles of diameter ~15–35 µm. All vessels had brisk blood flow immediately before cannulation and had no marginating white cells.

Solutions and Reagents

Mammalian Ringer solution was used for all dissections, perfusate and superfusate. The solution composition was (in mM) 132 NaCl, 4.6 KCl, 1.2 MgSO$_4$, 2.0 CaCl$_2$, 5.0 NaHCO$_3$, 5.5 glucose, and 20 HEPES. Its pH was balanced to 7.4 by adjusting the ratio of HEPES acid to base. In addition, the perfusate into the microvessel lumen contained bovine serum albumin (BSA, Sigma) at 10 mg/ml (1% BSA-Ringer solution). 4, 5-Diaminofluorescein diacetate (DAF-2 DA), N^G-monomethyl-L-arginine (L-NMMA), and sodium nitroprusside (SNP) were purchased from Sigma (Sigma-Aldrich, St. Louis, MO). The stock solutions of DAF-2 DA (10 mM) were prepared with 100% DMSO. The final concentrations of DAF-2 DA (5 µM), L-NMMA (1 mM) and SNP (50 mM) were achieved by dilutions of the stock with 1% BSA-Ringer solution [49]. FITC conjugated mouse anti-human heparan sulfate (Anti-HS, 10e4 epitope) was purchased from the United States Biological (Swampscott, MA). It was diluted to 1:50 (20 µg/ml) in 1% BSA-Ringer solution for labeling heparan sulfate in the microvascular

endothelial surface glycocalyx. Alexa Fluor 488-labeled Griffonia (Bandeiraea) Simplicifolia Lectin II (GSL II) (Vector Labs, USA) at 40 µg/ml in 1% BSA-Ringer solution was used to recognize chondroitin sulfate. Hyaluronic acid binding protein (Millipore EMD) was first conjugated with Alexa Fluor 488 following a labeling kit from Invitrogen (Cat# A20181). Then Alexa Fluor 488-labeled hyaluronic acid binding protein at 50 µg/ml in 1% BSA-Ringer solution was used to label hyaluronic acid. A blocking solution was made of 5% goat serum (Invitrogen, Eugene, OR) in 1% BSA-Ringer. *F. heparinum* Heparinase III (50 mU/ml, IBEX, Canada) is selectively active only towards heparan sulfate (HS) [53]. All of the solutions described above were made at the time when the experiment was performed and were discarded at the end of the day.

Intravital Microscopy

A Nikon Eclipse TE2000-E inverted fluorescent microscope was used to observe the mesentery. The tissue was observed with either transmitted white light from a light pipe suspended above the preparation or with fluorescent light from an illumination system (the monochromator with a xenon lamp FSM150Xe, Bentham Instrument Ltd., UK). The monochromator can generate the light of wavelength from 200 to 700nm. The observation of the DAF-2 labeled microvessel wall and that of fluorescently labeled glycocalyx were done by a high-performance digital 12-bit CCD camera (SensiCam QE, Cooke Corp., Romulus, MI, USA) with a Super Fluor 20x objective lens (NA = 0.75, Nikon) and recorded by InCyt Im^{TM} imaging and analyzing system (Intracellular Imaging Inc., Cincinnati, OH, USA). The excitation/emission wavelength (nm) were 485/538 nm and 490/525nm for DAF-2 and FITC, respectively.

Determination of Perfusion Velocity in a Microvessel

Fluorescent polystyrene microspheres (3 µm diameter, Phosphorex, Inc., Hopkinton, MA) were used to measure perfusion flow velocity in a microvessel [54]. The excitation/emission wavelength for the fluorescent beads was 468/510 nm (green). The bead movement was monitored by a high performance analog 10 bit XR/MEGA-10 ICCD camera (Stanford Photonics Inc. CA) and recorded on VCR tapes. The recorded analog video images were first converted into digital movies (640×480 µm/frame at 30 frames/s under medium/low video profile) via the Microsoft media encoder (Microsoft, Seattle, WA). From the digital movies, the images of bead movement were taken by the Microsoft Live Movie Maker (Microsoft, Seattle, WA), and analyzed by NIH Image-J to determine its centerline velocity. Mean velocity in that vessel was then calculated using the correction 1/1.6 of the centerline bead velocity [55,56].

Perfusion of a Single Microvessel under Low and High Flow Velocities

A single microvessel was cannulated with a glass micropipette (~15–30 µm tip diameter, World Precision Instrument Inc., Florida) and perfused with specific solutions. An initial pressure of 15–20 cmH$_2$O for the post-capillary venules, or 20–30 cmH$_2$O for the arterioles, was applied through the pipette to the microvessel lumen from a water manometer connected to the pipette holder. The initial pressure was set to balance the downstream blood pressure. Then the pressure was increased to a perfusion pressure. The difference between the initial pressure and the perfusion pressure was denoted as the driving pressure. The perfusion flow velocity was determined by the driving pressure and was calculated from the movement of a 3 µm fluorescent bead. The relationship between driving pressure and perfusion velocity is demonstrated in Fig. 1 for 3 vessels of typical sizes. As shown in Fig. 1, for a reduced (low) flow of ~ 300 µm/s, the driving pressure was set around 0.5 cmH$_2$O; for a normal (high) flow in a
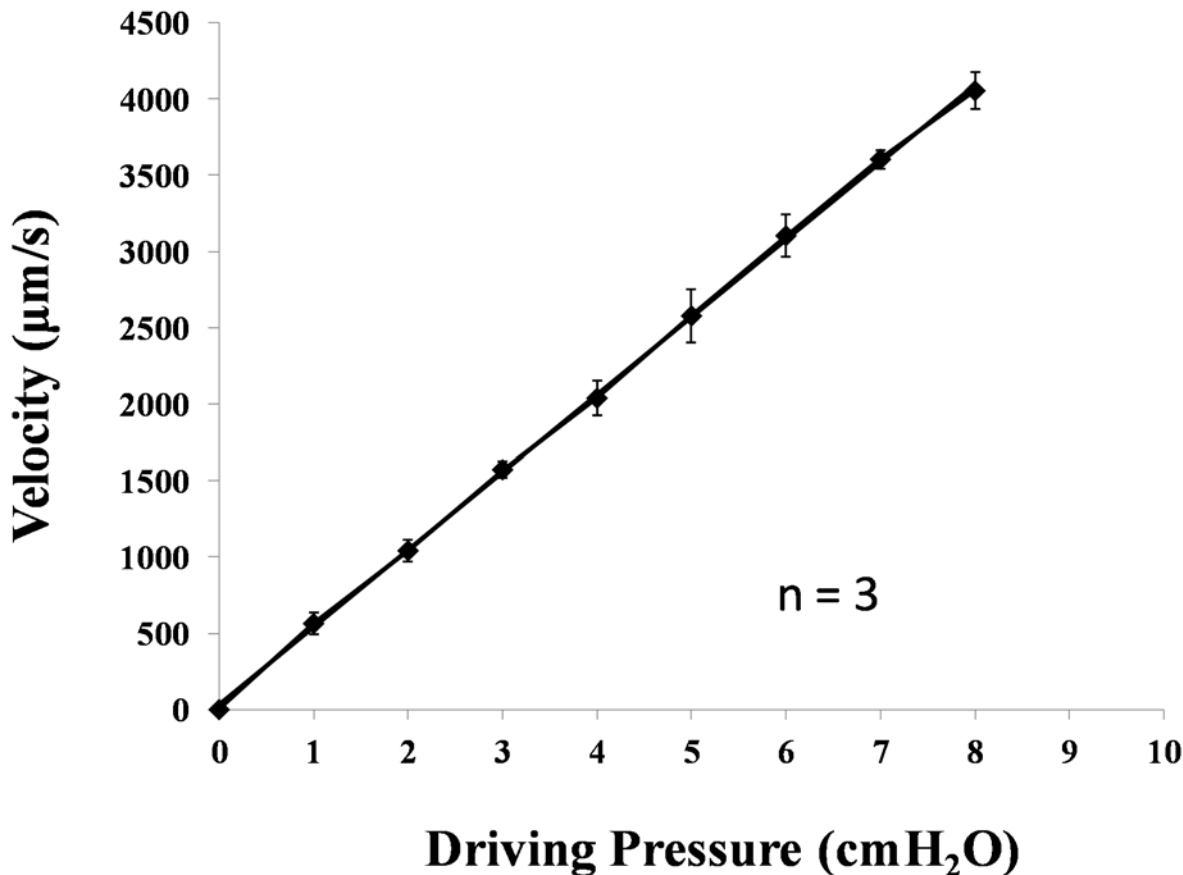
Figure 1. Mean perfusion flow velocity as a function of the driving pressure. The perfusion flow velocity was determined by tracking the movement of a fluorescent bead of 3 μm diameter when the vessel was cannulated and perfused at a known driving pressure measured from a water manometer. The movement of a fluorescent bead was recorded using our imaging system at various pressures for each vessel. Three vessels were tested and values shown are mean ± SE.

post-capillary venule (~1000 μm/s) and in an arteriole (2000–2500 μm/s) [54], the driving pressure was set around ~2 cmH$_2$O and 4–5 cmH$_2$O, respectively.

If we assume Hagen-Poiseuille flow in a microvessel (Reynolds number is in the order of 0.01 in these mesenteric microvessels), the wall shear stress is given by $(8\mu V_{mean})/D$, where μ is the viscosity of the perfusate, which is 9.5×10^{-3} dyn.s/cm^2 for 10 mg/ml BSA Ringer at 37°C [57], V_{mean} is the mean perfusion velocity (Fig. 1) and D is the vessel diameter. For the microvessels used in this study, the low flow of V_{mean} ~300 μm/s represents a mean wall shear stress of ~ 0.6 dyn/cm^2 in a post-capillary venule and ~ 0.8 dyn/cm^2 in an arteriole. The high flow of ~1000 μm/s represents a mean wall shear stress of ~2 dyn/cm^2 (range1.9–2.2) in a post-capillary venule and the high flow of 2000–2500 μm/s represents a mean wall shear stress of ~6.2 dyn/cm^2 (range 5.1–7.6) in an arteriole.

Measurement of Endothelial NO Production in a Microvessel

The method used to measure NO production in the endothelial cells forming the microvessel wall was similar to that described in [49]. Endothelial NO levels were visualized in individually perfused microvessels using DAF-2 DA, a membrane permeable fluorescent indictor for NO, and a fluorescence imaging system. Briefly, in each experiment, a microvessel was cannulated and loaded with DAF-2 DA (5 μM) in 1% BSA-Ringer solution for 45 min at a perfusion

velocity <300 μm/s. Then, focused on the mid-plane of the vessel wall, the image was first collected for 10 min at a low flow of ~300 μm/s and switched to a normal (high) flow of ~1000 μm/s for a post-capillary venule, or 2000–2500 μm/s for an arteriole by adjusting the perfusion pressure in a water manometer. The image was collected for 60 min under the high flow. To inhibit the eNOS activity, 1 mM L-NMMA was present during the loading, low and high flow periods. To degrade the ESG, the microvessel was pretreated for 1 h at a low flow with 50 mU/mL *F. heparinum* heparinase III. To test if the endothelial cells forming the microvessel wall were damaged by the enzyme treatment, the superfusate of a NO donor, sodium nitroprusside (SNP), was applied at the end of the experiment.

All images of endothelial DAF-2 were analyzed with the public domain National Institutes of Health IMAGE J program by selecting a region of interest (ROI) focused on the mid-plane of the vessel wall. ROI has a length of ~200–500 μm and a width of a vessel diameter. The baseline of the NO production (DAF-2 intensity), F_0, was chosen as that at 45 min after DAF-2 DA loading; flow-induced temporal changes in DAF-2 intensity were expressed as $F(t)/F_0$ for each vessel, where $F(t)$ is the DAF-2 intensity at time t.

The fluorescence chemical formation of DAF-2 by NO is irreversible [58] and the detected NO-sensitive fluorescence with DAF-2 represents a cumulative production of NO. The DAF-2 fluorescence intensity vs. time curve was fit by a sigmoidal four-parameter Gompertz growth model for the NO production function $f(t)$ [59]

$$f(t) = a \times \exp\left(-\exp\left(-\frac{t-t_0}{b}\right)\right) + c \qquad (1)$$

where a, b, c and t_0 are the fitting constants, which were determined by SigmaPlot 11.2 through curve fitting the measured data. Equation 1 is an empirical formula used to describe the transient NO production under chemical stimuli [49,59,60]. From Equation 1, the NO production rate was calculated as

$$\frac{df}{dt} = \frac{a}{b} \times \exp\left(-\left(\exp\left(-\frac{t-t_0}{b}\right) + \frac{t-t_0}{b}\right)\right) \qquad (2)$$

Immuno-Labeling and Quantification of Microvessel Endothelial Surface Glycocalyx (ESG)

To quantify the ESG of the microvessel wall, FITC-conjugated HS antibody was used to label HS, the most abundant glycosaminoglycan forming the endothelial surface glycocalyx (ESG) [4,61]. Similar to our previous study [17,50], a post-capillary venule of rat mesentery was cannulated by a θ micropipette. The upper surface of the mesentery was continuously superfused by a dripper with mammalian Ringer solution at 4 °C, which was regulated by a controlled water bath with ice and monitored using a thermometer probe. The vessel was first perfused for 15 min with a blocking solution of 5% goat serum containing 1% BSA-Ringer through one lumen of θ pipette. Then the perfusion was switched to another lumen of the pipette to inject FITC-conjugated anti-heparan sulfate (HS) in 1%BSA-Ringer (20 μg/ml) into the microvessels for ~2.5 h. The 2.5 h was long enough to allow FITC-anti-HS to infiltrate the entire depth of the ESG. After 15 min perfusion of the first perfusate to wash away the free dye, the vessel with fluorescently labeled glycocalyx (focused at the mid-plane of a vessel) was imaged by the same imaging system used in the NO measurement. The intensity of the fluorescently labeled glycocalyx in the vessel segment was measured by InCyt Im^TM imaging and analyzing system (Intracellular Imaging Inc., Cincinnati, OH, USA). To test the assumption that the fluorescence

intensity is linearly related to the amount of the fluorescently labeled glycocalyx, we did *in vitro* calibration experiments. We used the same instrument settings in the calibration experiments as those used in the *in vivo* measurement of the fluorescently labeled glycocalyx. The linear range of FITC-anti-HS concentrations was from 0 to 50 μg/ml under our settings. We thus chose 20 μg/ml FITC-anti-HS in our experiments. We determined the amount of the fluorescently labeled glycocalyx in the vessels under control and after 1 h treatment with 50 mU/mL *F. heparinum* heparinase III, the same dosage and treatment time as for the NO measurement.

By turning on the fluorescent light under the bright field, we can observe the microvessel boundary and determine the location of FITC-anti-HS labeled ESG. We can see the FITC-anti-HS labeled ESG at the luminal side of the microvessel wall under our microscope and the fluorescent region is almost completely gone after the enzyme treatment. Since anti-HS antibody is a macromolecule of MW ~150kD and takes a couple of hours to penetrate the ESG under 4°C [50], it is very hard to cross the microvessel wall to label the matrix components at the abluminal side of the vessel wall.

To investigate if there is any CS and HA in arterioles, we used the same immunolabeling protocol with Alexa Fluor 488 conjugated GSL II and hyaluronic acid binding protein to recognize CS and HA of ESG. We did not observe either CS or HA in arterioles of rat mesentery.

Measurement of Microvessel Diameters

Images of microvessels collected by the CCD camera were inputted into IMAGE J program and the diameter of a vessel was determined by the distance between the outer walls of the vessel. Diameters were measured at 3 locations of each vessel. The averaged value was the diameter for that vessel.

Data Analysis

Data are presented as mean ± SE, unless indicated otherwise. Statistical analysis was performed by two-way (time and cumulative NO level) ANOVA using Sigma Plot 11.2 from Systat Software Inc. (San Jose, CA). A level of $p < 0.05$ was considered a significant difference in all experiments.

Results

Flow-Induced NO Production and Its Regulation by Endothelial Surface Glycocalyx in Post-capillary Venules

Fig. 2 demonstrates typical DAF-2 images of post-capillary venules under various conditions. The left Fig. in each panel shows the image at 10 min after low flow and the right one shows that the image at 60 min after high flow. Fig. 3 plots the normalized DAF-2 fluorescence intensity, $F(t)/F_0$, under the low (~300 μm/s) and high (~1000 μm/s) perfusion velocities. The baseline intensity F_0 is that after 45 min DAF-2 DA loading for each vessel (t = 0 in Fig. 3). The solid line with diamonds is for the control with the perfusate of 1% BSA Ringer; the dashed line with squares is for the 1 h pretreatment of heparinase III; the dotted line with crosses is for that in the presence of an eNOS inhibitor, L-NMMA, and the dash-dot-dash line with triangles is for the sham control under low flow only. We can see from Fig. 3, 10 min low flow insignificantly increased the NO-DAF-2 by less than 5% under all the conditions ($p > 0.05$). After switching to the high flow, NO-DAF-2 was not significantly increased until 15 min later for the control and for that in the presence of L-NMMA ($p < 0.03$). After 15 min high flow, NO-DAF-2 increased to 1.27 ± 0.04-fold of its baseline, NO continuously increased under the high flow, reaching a plateau in ~50 min, and to 1.53 ± 0.04-fold in 60 min (n = 9). Inhibition of eNOS by
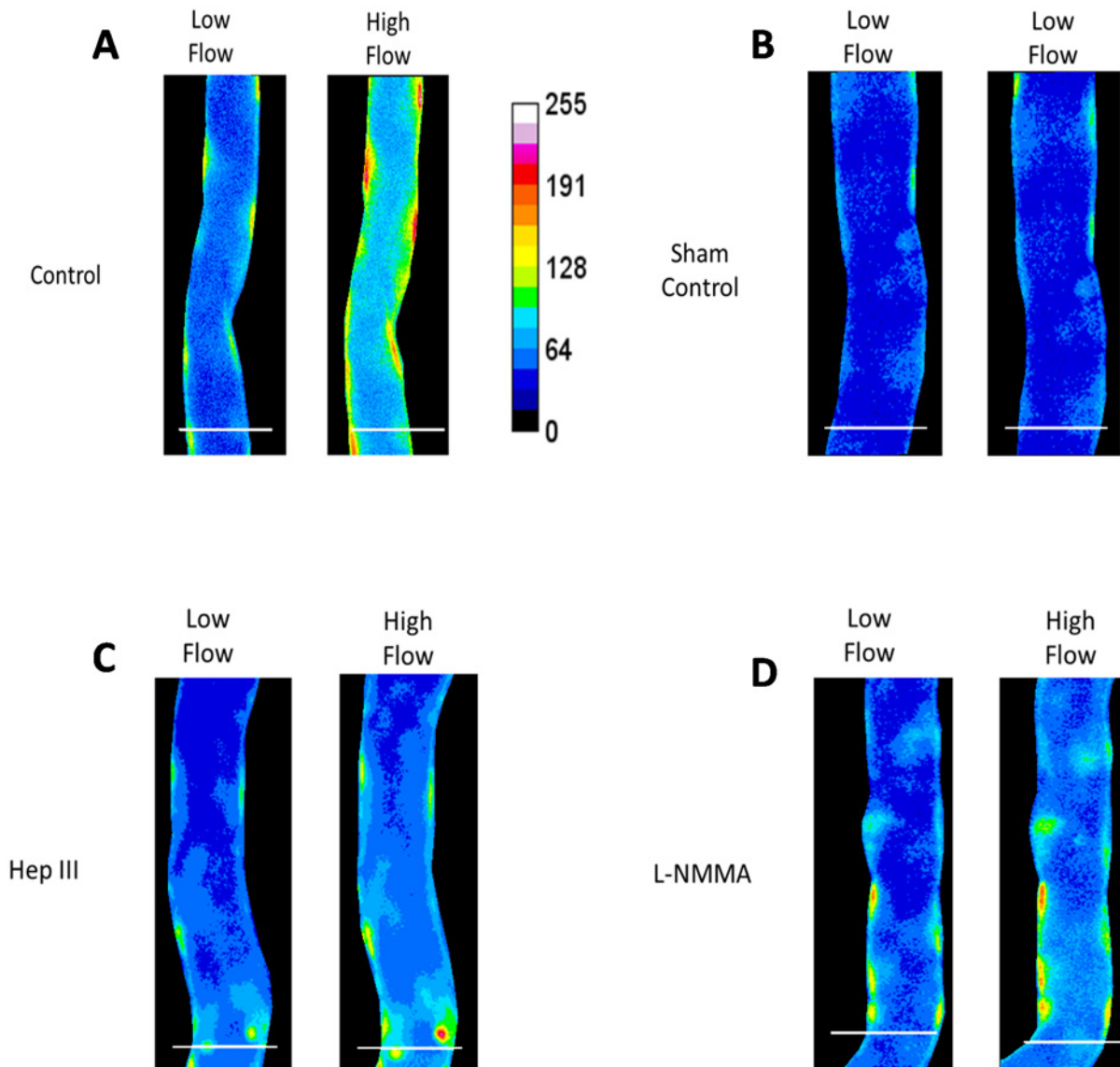
Figure 2. Representative DAF-2 fluorescence images for post-capillary venules. Images were taken after 10 min low flow (left panel) and an additional 60 min high flow (right panel). A) control (1% BSA Ringer); B) sham control (low flow over entire time); **C)** 1 h pretreatment of heparinase III; and **D)** in the presence of L-NMMA. Scale bar is 50 μm.

1 mM L-NMMA attenuated the flow-induced NO increase to 1.13 ± 0.01-fold in 15 min (p = 0.018 compared to the control) and 1.30 ± 0.03-fold in 60 min (p < 0.001 compared to the control, n = 6), respectively.

In contrast, the flow-induced NO production was almost completely abolished by the 1 h pretreatment with 50 mU/mL heparinase III (n = 6) (p > 0.07). To examine if the enzyme treatment damaged the endothelial cells and to verify that the endothelial cells in each vessel were well loaded with DAF-2, at the end of the 60 min high flow, a NO donor, sodium nitro-prusside (SNP), was applied to the superfusate and a large sudden increase in the NO-DAF-2 fluorescence intensity was observed in each vessel (data not shown). If endothelial cells are damaged, the loaded DAF-2 in their cytoplasm would be out and washed away by the perfus-ate, adding the NO donor, SNP, would not induce the fluorescence in individual endothelial
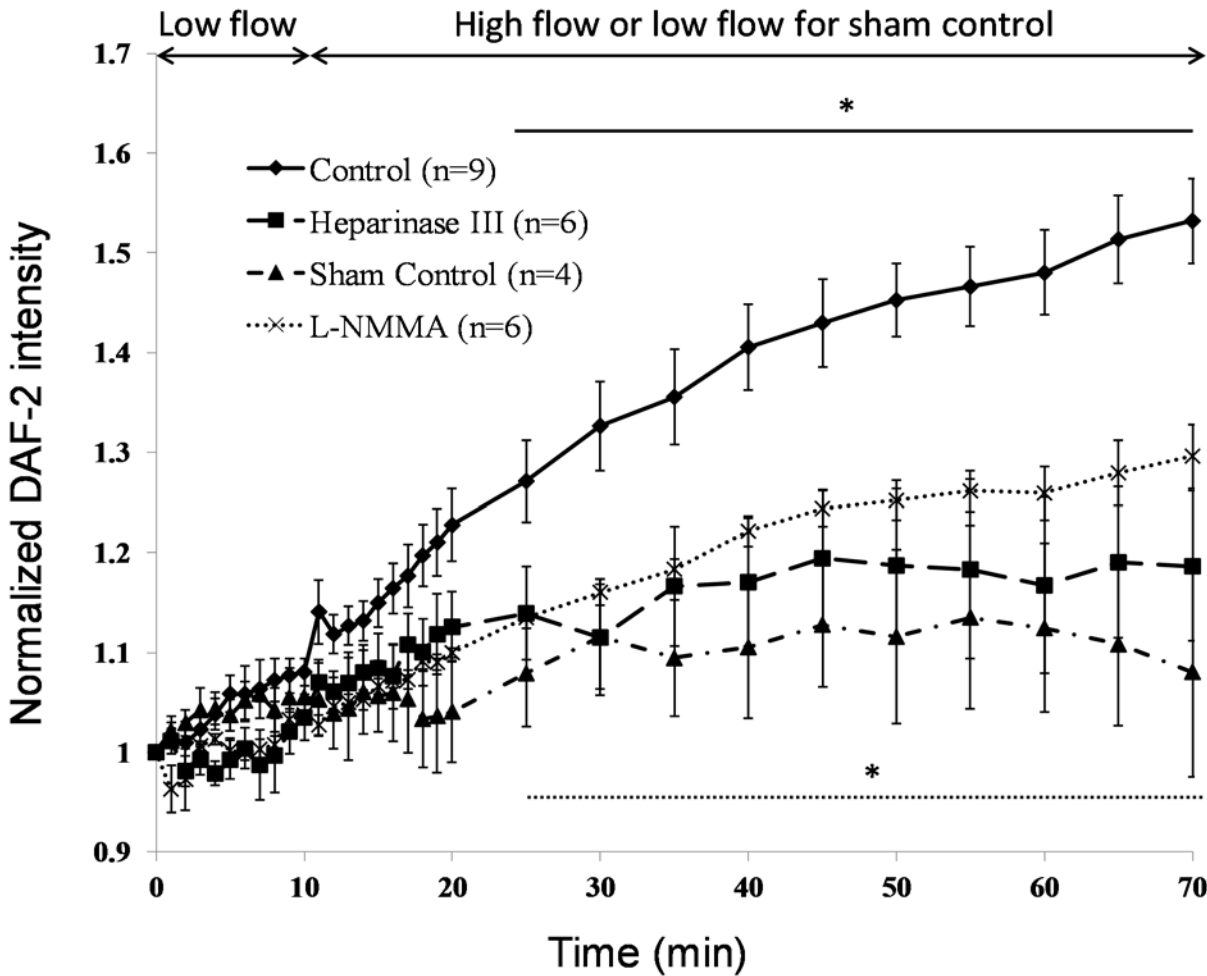
Figure 3. Flow-induced increases in NO production (DAF-2 intensity normalized by that after 45min DAF-2 DA loading) under various conditions in post-capillary venules. The solid line with diamonds is for the control perfusing 1% BSA-Ringer under the low flow (~300 μm /s) for 10 min and the high flow (~1000 μm/s) for 60 min; the dash-dot-dash line with triangles is for the sham control perfusing 1% BSA-Ringer under the low flow for 70 min; the dashed line with squares is for that with 1 h pretreatment of heparinase III; and the dotted line with crosses is for that in the presence of L-NMMA. * p < 0.05 compared with that at 10 min low flow (for the control and L-NMMA treatment).

cells forming the vessel wall. Therefore superfusion of SNP is widely used to test if endothelial cells forming the microvessel wall are damaged by the treatment [49,60]. Prior permeability study also reported that 1 h treatment with 50 mU/mL heparinase III did not change other components of the microvessel wall except degrading the ESG [17].

After curve fitting using Equation 1 for the normalized DAF-2 intensity, $F(t)/F_0$, we obtained the normalized NO production function f(t). Its derivative, Equation 2, gives the NO production rate df/dt. In Fig. 4, we plotted both NO production (the symbols for the measured data and the solid line for the fitting curve) and the production rate (dashed line). This sigmoidal four-parameter Gompertz growth model fit very well for the flow-induced NO production data with $R^2 > 0.97$ for all the cases except for the sham control when there was no NO generated. Fig. 4A is for the control case by perfusing 1%BSA Ringer under low and high flows. Different from the sudden and transient increase in the NO production by chemical stimuli such as bradykinin [59] and platelet-activating factor (PAF) [60], the flow-induced NO production was gradual and the highest NO production rate occurred at about 5 min after switching to the
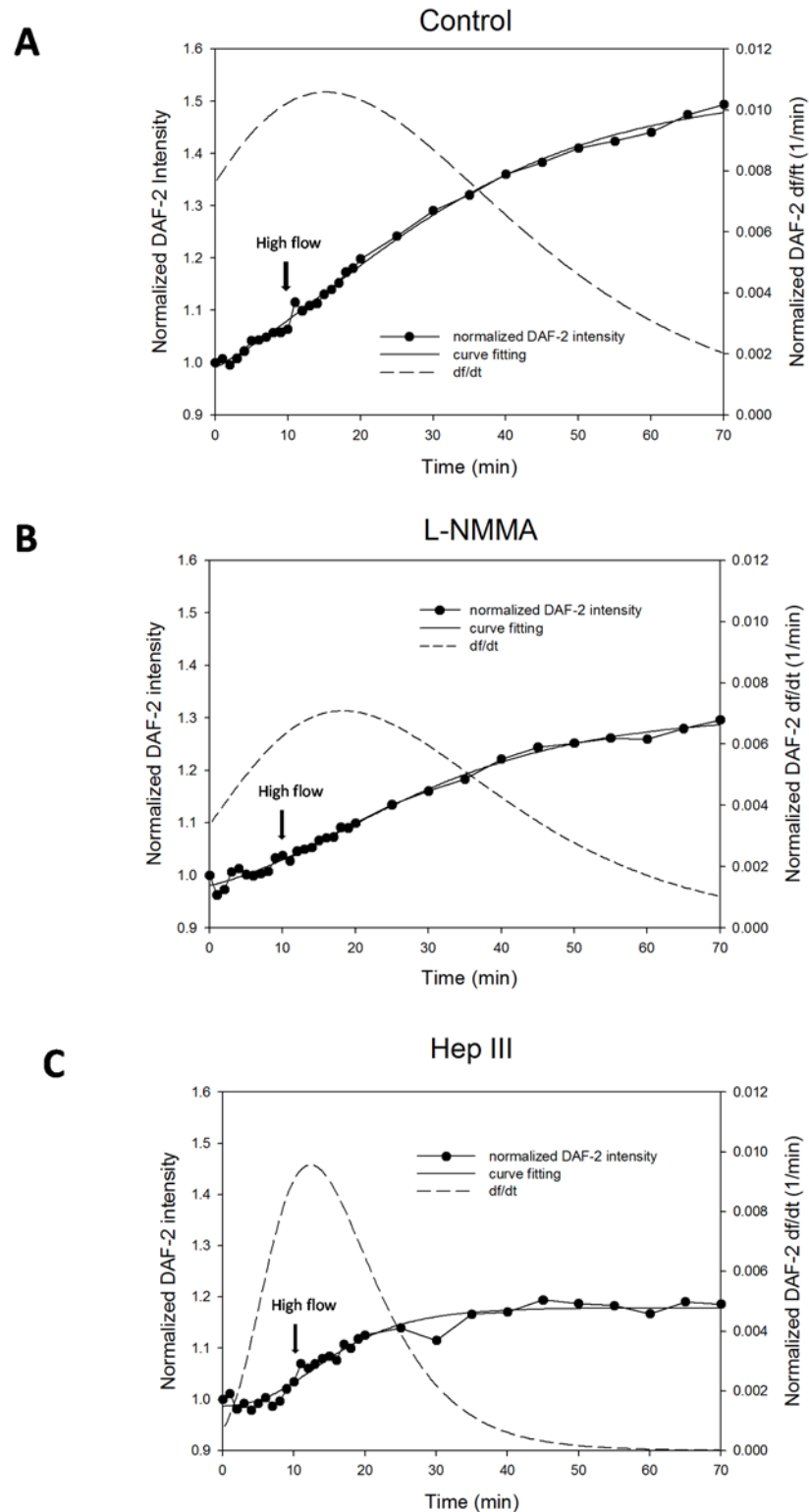
Figure 4. Curve fitting for the flow-induced increases in NO production (DAF-2 intensity normalized by that after 45min DAF-2 DA loading) (smooth solid line) and production rate (df/dt) (dashed line) in post-capillary venules. A) control (1% BSA Ringer); B) in the presence of L-NMMA; and C) 1 h pretreatment of heparinase III. The filled circles are the measured data.

doi:10.1371/journal.pone.0117133.g004

high flow, which was ~0.01/min. After the peak, the endothelial cells continued to produce NO at a slower rate. Inhibition of eNOS by L-NMMA attenuated the NO production, reduced the production rate but did not change the temporal pattern of the NO production by the flow (Fig. 4B). On the contrary, enzymatic degradation of ESG altered the NO production pattern by the flow. Fig. 4C shows that after 1h pretreatment of heparinase III, the flow-induced NO production increase was sudden and transient, similar to that observed by applying brady-kinin [59] and PAF [60]. Interestingly, the peak production rate after the enzyme treatment, ~0.01/min, was the same as that without enzyme treatment.

Heparan Sulfate ESG Removal by Heparinase III

To examine the removal of the ESG, we did the immunostaining of heparan sulfate (HS) before and after the enzyme treatment in individual post-capillary venules. Fig. 5 indicates that 1 h 50 mU/mL heparinase III treatment removed more than 80% of the ESG (p < 0.001).

Flow-Induced NO Production in Arterioles

In our previous study [50], we could not observe significant HS in arterioles although we found significant HS in capillaries and post-capillary venules of rat mesentery. In the current study, we also performed immunolabeling of chondroitin sulfate (CS) and hyaluronic acid (HA) in the arterioles. No significant CS or HA was found in arterioles. To examine if the flow can also induce NO production in mesenteric arterioles in the absence of ESG, we measured NO production in arterioles. Fig. 6 demonstrates the results, which are similar to those observed in post-capillary venules. We raised the high flow perfusion velocity to ~2000–2500 μm/s, which is the mean blood flow velocity in mesenteric arterioles [54]. After switching to the high flow, NO-DAF-2 was not significantly increased until 20 min later for the control and until 35 min later for that in the presence of L-NMMA (p <0.05). After 20 min high flow, NO-DAF-2 increased to 1.20 ± 0.02-fold of its baseline, NO continuously increased under the high flow, reached a plateau in ~50 min, and to 1.48 ± 0.05-fold in 60 min. Inhibition of eNOS by 1 mM L-NMMA attenuated the flow-induced NO increase to 1.19 ± 0.03-fold (p < 0.001) in 60 min.

In parallel with the post-capillary venules, in Fig. 7, we plotted both NO production (the symbols for the measured data and the solid line for the fitting curve) and the production rate (dashed line). The sigmoidal four-parameter Gompertz growth model also fitted very well for the flow-induced NO production data in arterioles with $R^2 > 0.95$. Fig. 7A is for the control case by perfusing 1%BSA Ringer under low and high flows and Fig. 7B for that in the presence of L-NMMA. Similar to that in the post-capillary venules, the flow-induced NO production was gradual and the highest NO production rate occurred at about 20 min after switching to the high flow, which was ~0.01/min. After the peak, the endothelial cells continued to produce NO at a slower rate. Inhibition of eNOS by L-NMMA attenuated the NO production, reduced the production rate but did not change the temporal pattern of the NO production by the flow.

Flow-Induced NO Production Does Not Change the Diameter of Microvessels

As a vasodilator, NO induced by flow may increase the size of microvessels. We examined the vessel diameters right after 45 min DAF-2 DA loading, at 10 min low flow and at 60 min high flow. Tables 1,2 show that the mean diameters of both post capillary venules and arterioles have no significant changes under all conditions in our experiments (p > 0.7).
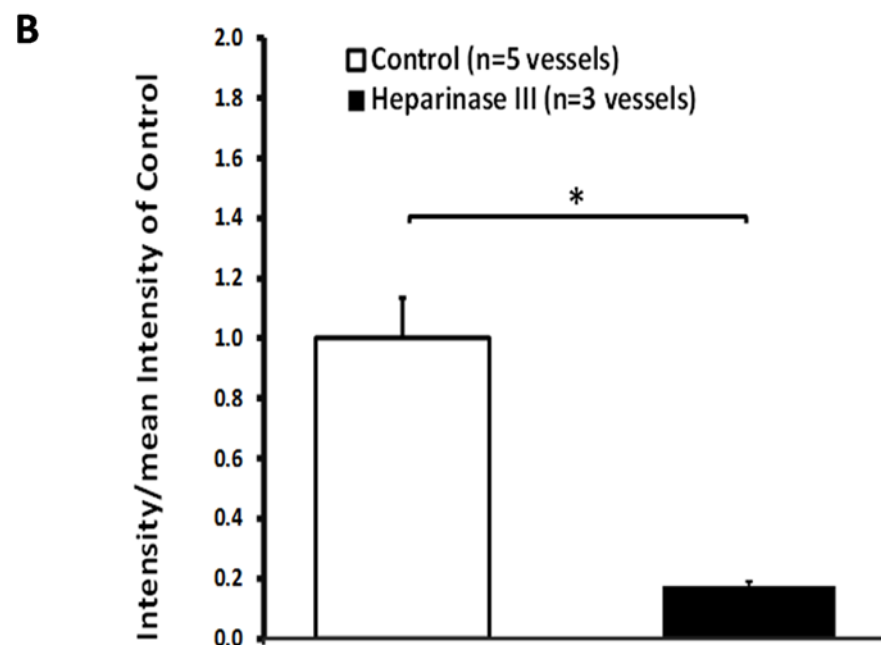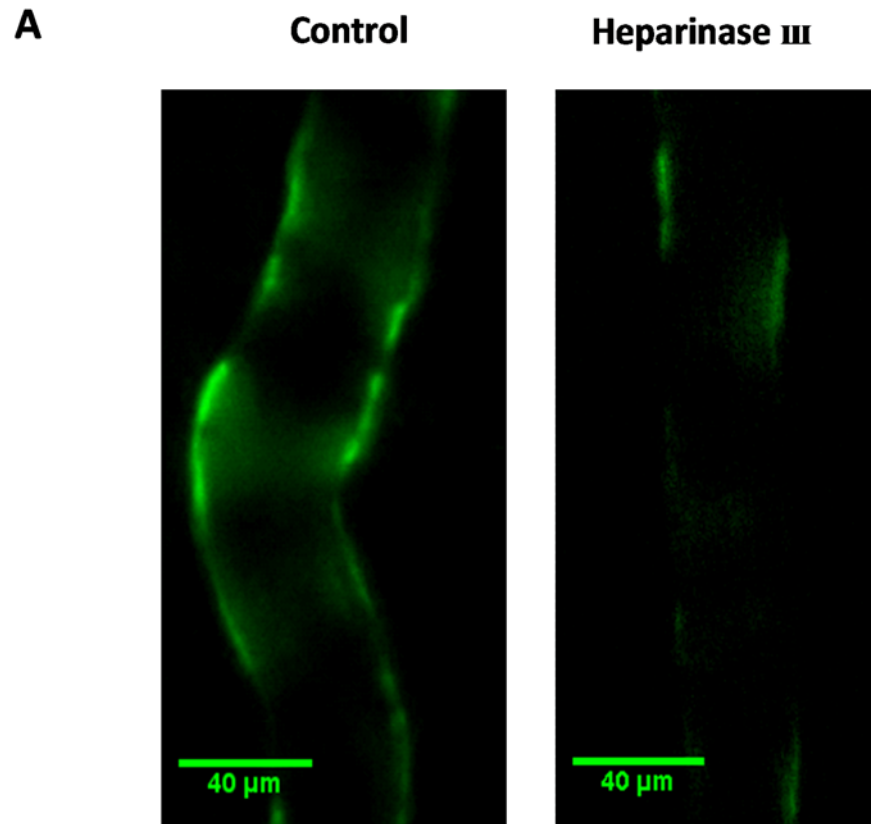
Figure 5. Images of fluorescently labeled heparan sulfate in a control vessel (left in Fig. 5A) and a vessel treated with heparinase III for 1 h (right in Fig. 5A). Fig. 5B shows the comparison of the intensity of the fluorescently labeled heparan sulfate in 5 control vessels and that in 3 heparinase III treated vessels. * p < 0.001.
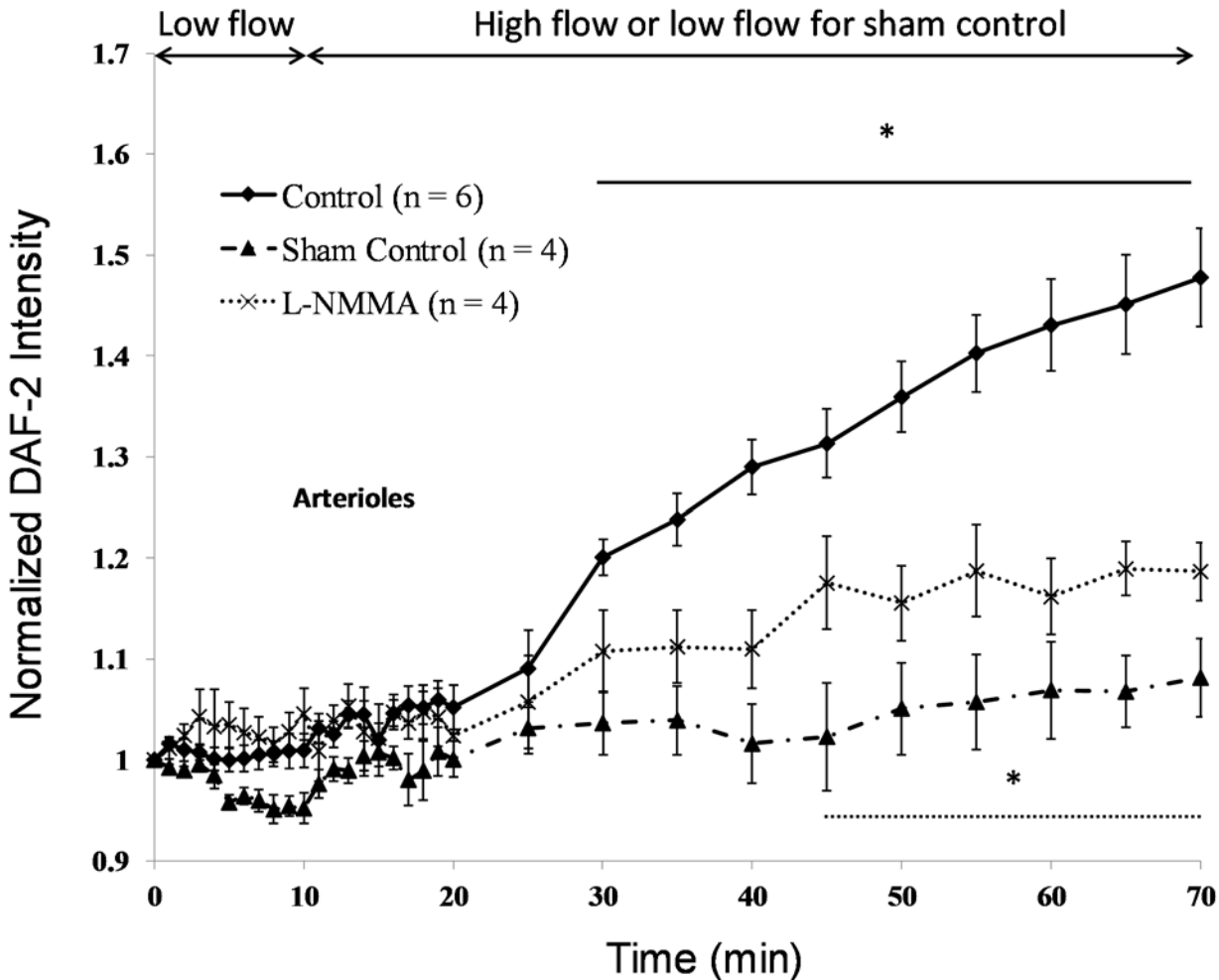
Figure 6. Flow-induced increases in NO production (DAF-2 intensity normalized by that after 45min DAF-2 DA loading) under various conditions in arterioles. The solid line with diamonds is for the control of perfusing 1% BSA-Ringer under the low flow (~300 μm/s) for 10 min and the high flow (~2000–2500 μm/s) for 60 min; the dash-dot-dash line with triangles is for the sham control of perfusing 1% BSA-Ringer under the low flow for 70 min; and the dotted line with crosses is for that in the presence of L-NMMA. * $p < 0.05$ compared with that at 10 min low flow (for the control and L-NMMA treatment).

doi:10.1371/journal.pone.0117133.g006

Discussion

Fluorescent images of DAF-2-loaded microvessels provide a direct visualization and quantification approach for analyzing the spatial and temporal NO production in ECs of intact microvessels [49,60]. Cannulation and perfusion of a single microvessel enable us to control the vessel flow rate properly [17,52]. In vivo perfusion of enzyme and immunostaining of the ESG in an individual microvessel enable us to more precisely degrade and quantify the specific ESG component [17,50]. By using these recently developed techniques in our and other labs, we demonstrated in the current study that degradation of the ESG at the post-capillary venule, specifically the HS component of the ESG, inhibited the flow-induced NO production in the ECs forming the microvessel wall, suggesting that the ESG plays a major role in mechano-sensing and transducing in microvessels. This is consistent with previous studies in cultured EC monolayers [21,27,28] and in arteries [42,43].
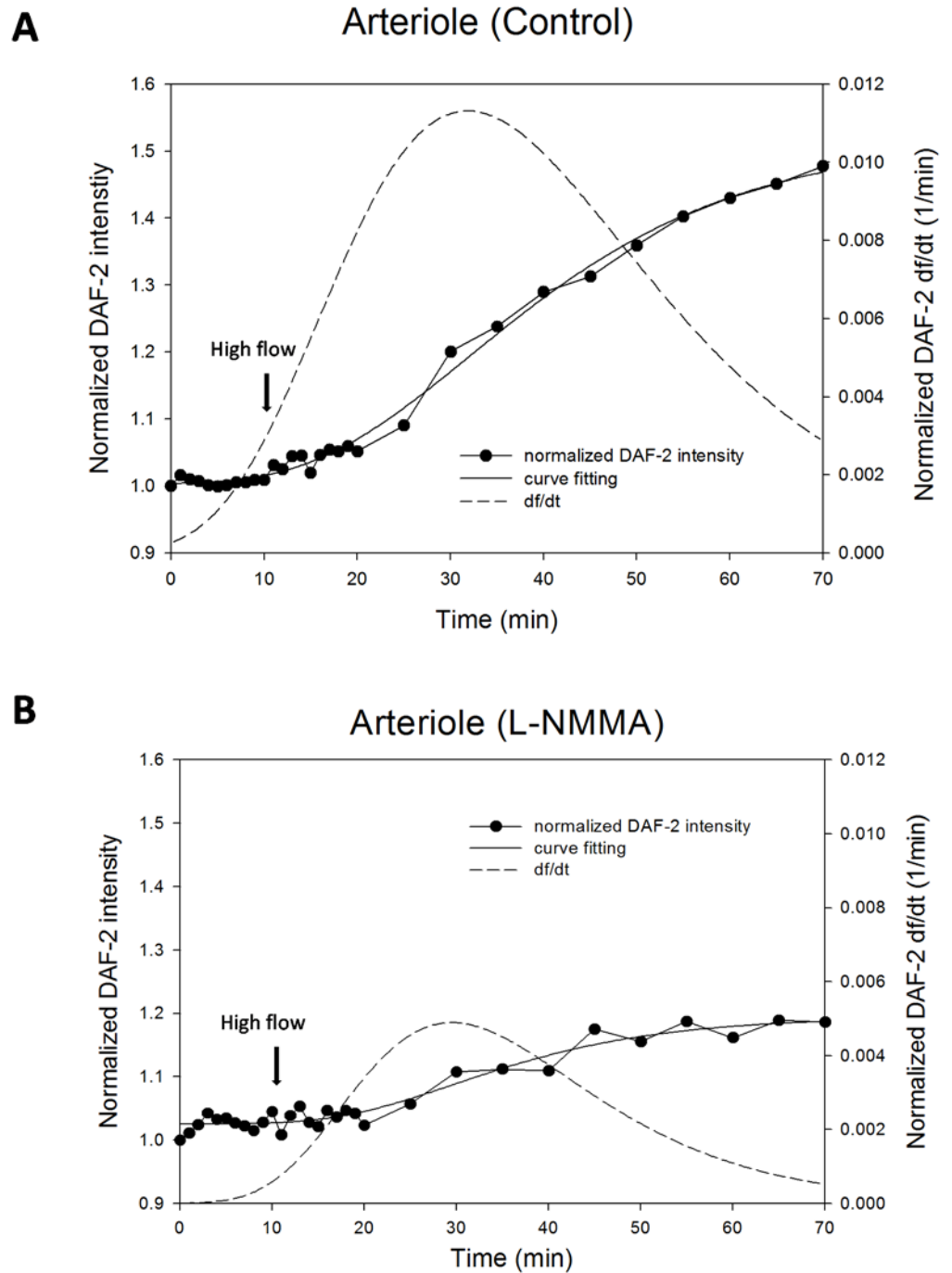
Figure 7. Flow-induced increases in NO production (DAF-2 intensity normalized by that after 45min DAF-2 DA loading) and production rate (df/dt) in arterioles A) control (1% BSA Ringer); B) in the presence of L-NMMA. The filled circles are the measured data, the solid line is the fitting curve and the dashed line is the production rate.

Table 1. Diameters of post-capillary venules under low (~300 μm/s) and high (~1000 μm/s) flows.

	0 min Low Flow	10 min Low Flow	60 min High Flow
Control (n = 9)	37.01 ± 2.71	37.47 ± 2.86	39.56 ± 2.71
Heparinase III (n = 6)	34.70 ± 3.41	34.76 ± 3.41	34.68 ± 3.24
L-NMMA (n = 6)	32.97 ± 1.38	32.87 ± 1.40	33.15 ± 1.39
Sham control (n = 4)	34.48 ± 3.67	34.20 ± 3.70	34.62 ± 3.60 (low flow)

Data shown are Mean ± SE (μm). $p > 0.7$.

doi:10.1371/journal.pone.0117133.t001

When exposing human umbilical vein endothelial cells (HUVECs) to steady laminar flow, Kuchan and Frangos [26] observed a biphasic response in NO production, with an initial burst of NO production within minutes followed by a gradual NO release over hours. It was also demonstrated that the initial rapid NO release was G protein and Ca^{2+} dependent but the later slower response was G protein and Ca^{2+} independent and shear level dependent [26]. A similar biphasic response of NO production was observed in BAECs when exposed to step changes in shear stress [21,62]. An NOS inhibitor, N^G-amino-L-arginine (L-NAA), completely blocked the flow-mediated NO release in HUVECs [26]. In the intact post-capillary venules, we did not observe a rapid NO production when switching to the high flow (Fig. 3). Instead, the NO production was rather gradual, though at a higher production rate in the beginning after switching to the high flow, which peaked around 5 min after the onset of high flows (Fig. 4). Enzymatic degradation of the HS completely inhibited the flow-generated NO production in intact post-capillary venules (Fig. 3,4c). In the presence of eNOS inhibitor, L-NMMA, the NO production in response to the flow was attenuated significantly (Figs. 3,4), suggesting that the flow-induced NO production is through activation of eNOS. L-NMMA is a relatively non-selective inhibitor of all NOS isoforms and is claimed to be a potent eNOS inhibitor. The current results showed that enzymatic degradation of ESG was a better inhibitor of the flow-induced NO production by endothelial cells.

The molecular mechanisms by which ESG regulates flow-induced NO production in the microvessel wall are not yet known. One possibility is a glypican-caveolae-eNOS mechanism. The transmembrane syndecans and the membrane bound glypicans are the major core protein families of heparan sulfate proteoglycans found on the EC plasma membrane [2,63]. Glypicans, to which HS binds, are linked to caveolae where eNOS resides [2]. When flow imposes drag force on HS, the mechanical stimuli would be transmitted via the glypican to the caveolae and trigger the NO production by eNOS inside the caveolae. This has been demonstrated recently in BAECs where it was shown that glypican-1 not syndecan-1 is the proteoglycan core protein mediating eNOS activation by shear stress [64].

Prior studies showed that 30 min treatment with 60 mU/ml heparinase III removed 60% of the HS in the ESG of BAEC monolayers [47] and 10 min treatment with 50 mU/ml heparinase III only reduced the ESG thickness by 57% in the post-capillary venule of rat mesentery [65].

Table 2. Diameters of arterioles under low (~300 μm/s) and high (~2000–2500 μm/s) flows.

	0 min Low Flow	10 min Low Flow	60 min High Flow
Control (n = 6)	25.47 ± 3.26	26.53 ± 3.39	27.68 ± 3.48
L-NMMA (n = 4)	29.64 ± 2.24	29.81 ± 4.29	31.52 ± 1.51
Sham control (n = 4)	26.24 ± 1.81	27.18 ± 1.71	27.16 ± 2.21 (low flow)

Data shown are Mean ± SE (μm). $p > 0.7$.

doi:10.1371/journal.pone.0117133.t002

Our current study revealed that 1 h treatment with 50 mU/ml heparinase III removed more than 80% of the HS in post-capillary venules (Fig. 5). Previous studies using the same type of enzyme reported no other changes in the structural components of the microvessel wall except for degrading the ESG [17]. No reaction of the endothelial cells or any significant off target degradation of CS or HA in cultured cell monolayers were reported even at much higher doses [66]. Since HS is the dominant GAG of the EC glycocalyx [2], our enzyme treatment should degrade most of the ESG. Without the ESG, flow-induced mechanical stimuli such as shear stress can directly act on the EC plasma membrane. Although the cumulative NO production in the microvessel wall was not significantly increased by enhancing the perfusion flow rate after degradation of the ESG (Fig. 3), when switching to the high flow, the NO production rate increased immediately, similar to what has been observed by applying agonists, such as bradykinin in intact endothelium of coronary arteries [59] and PAF in intact post-capillary venules [60]. In BAECs, addition of bradykinin induced significant NO production that was not inhibited by pretreatment with heparinase III [21]. These results suggest that additional mechanisms in the absence of the ESG can also trigger NO production, by the potential mechano-sensors and transducers at the EC plasma membrane and within the EC cytoskeleton, e.g., cell adhesion molecules, G-protein-coupled receptors and G-proteins, actin filaments and integrins [4,34].

We previously observed a FITC-anti-HS labeled ESG layer of ~ 1 μm in capillaries and post-capillary venules of rat mesentery and a ESG layer of ~2 μm at rat aorta, but we did not observe significant HS in arterioles [50], and neither HA or CS in the current study. Without finding significant GAGs, we still observed flow-induced NO production in arterioles, and the flow-induced NO production was also attenuated by an eNOS inhibitor, L-NMMA (Fig. 6). These observations are consistent with findings of Williams [57] in frog mesenteric capillaries. She reported that pronase treatment, which completely degraded the glycocalyx, led to an enhanced sensitivity of endothelial hydraulic conductivity to shear stress that has been shown in other studies to be mediated by enhanced NO production [67]. This is also consistent with a study by Lopez-Quintero et al. [28] that showed that the sensitivity of NO production to shear stress was not inhibited when the glycocalyx was highly disrupted in protein-free media. In our study, when the ECs forming the arteriole wall are not covered by significant ESG, the flow-induced mechanical stimuli can directly act on the EC plasma membrane. Then other EC mechano-sensors and transducers may come into play to regulate vascular functions [4,34]. Additional studies will be required to unravel this puzzle and elucidate the functional mechanisms of ESG and various EC mechano-sensors and transducers mediating NO production in arterioles.

As a vasodilator, the flow-induced NO slightly increased the diameter of post-capillary venules and arterioles under control conditions without enzyme treatment and eNOS inhibition although the increase was not significant (p > 0.7, Tables 1,2). One reason is that we set up the high flow rate as the normal blood flow rate in respective microvessels, which does not require the reduction in the flow resistance by increasing the vessel size. Although the temporal patterns in the ESG mediated flow-induced NO production are different from those in agonist (PAF)-mediated NO production [60] in the same type of microvessels, the NO production vs. time curve by both factors satisfies the sigmoidal four-parameter Gompertz growth model, suggesting a common NO generation mechanism by which ECs respond to external stimuli. Further investigation is required to elucidate this common mechanism.

Acknowledgments

Author Contributions

Conceived and designed the experiments: BMF JMT. Performed the experiments: WY BC JY LZ MZ. Analyzed the data: WY BC BMF. Contributed reagents/materials/analysis tools: WY BC BMF. Wrote the paper: BMF WY JMT.

References

1. Barakat AI (2008) Dragging along: the glycocalyx and vascular endothelial cell mechanotransduction. Circulation research 102: 747–748. doi: 10.1161/CIRCRESAHA.108.174839 PMID: 18403731

2. Tarbell JM, Pahakis MY (2006) Mechanotransduction and the glycocalyx. Journal of internal medicine 259: 339–350. doi: 10.1111/j.1365-2796.2006.01620.x PMID: 16594902

3. Weinbaum S, Tarbell JM, Damiano ER (2007) The structure and function of the endothelial glycocalyx layer. Annual review of biomedical engineering 9: 121–167. doi: 10.1146/annurev.bioeng.9.060906.151959 PMID: 17373886

4. Fu BM, Tarbell JM (2013) Mechano-sensing and transduction by endothelial surface glycocalyx: composition, structure, and function. Wiley Interdisc Rev Syst Biol Med 5: 381–390. doi: 10.1002/wsbm.1211 PMID: 23401243

5. Becker BF, Chappell D, Jacob M (2010) Endothelial glycocalyx and coronary vascular permeability: the fringe benefit. Basic research in cardiology 105: 687–701. doi: 10.1007/s00395-010-0118-z PMID: 20859744

6. Curry FR, Adamson RH (2010) Vascular permeability modulation at the cell, microvessel, or whole organ level: towards closing gaps in our knowledge. Cardiovascular research 87: 218–229. doi: 10.1093/cvr/cvq115 PMID: 20418473

7. van den Berg BM, Vink H, Spaan JA (2003) The endothelial glycocalyx protects against myocardial edema. Circulation research 92: 592–594. doi: 10.1161/01.RES.0000065917.53950.75 PMID: 12637366

8. van Haaren PM, VanBavel E, Vink H, Spaan JA (2003) Localization of the permeability barrier to solutes in isolated arteries by confocal microscopy. American journal of physiology Heart and circulatory physiology 285: H2848–2856. PMID: 12907418

9. Constantinescu AA, Vink H, Spaan JA (2003) Endothelial cell glycocalyx modulates immobilization of leukocytes at the endothelial surface. Arteriosclerosis, thrombosis, and vascular biology 23: 1541–1547. doi: 10.1161/01.ATV.0000085630.24353.3D PMID: 12855481

10. Mulivor AW, Lipowsky HH (2009) Inhibition of glycan shedding and leukocyte-endothelial adhesion in postcapillary venules by suppression of matrixmetalloprotease activity with doxycycline. Microcirculation 16: 657–666. doi: 10.3109/10739680903133714 PMID: 19905966

11. Pries AR, Secomb TW, Gaehtgens P (2000) The endothelial surface layer. Pflugers Archiv: European journal of physiology 440: 653–666. doi: 10.1007/s004240000307 PMID: 11007304

12. Wu Q, Andreopoulos Y, Weinbaum S (2004) From red cells to snowboarding: a new concept for a train track. Physical Review Letters 93: 194501. doi: 10.1103/PhysRevLett.93.194501 PMID: 15600838

13. Chappell D, Heindl B, Jacob M, Annecke T, Chen C, et al. (2011) Sevoflurane Reduces Leukocyte and Platelet Adhesion after Ischemia-Reperfusion by Protecting the Endothelial Glycocalyx. Anesthesiology 115: 483–491. doi: 10.1097/ALN.0b013e3182289988 PMID: 21785339

14. Reitsma S, Slaaf DW, Vink H, van Zandvoort MA, oude Egbrink MG (2007) The endothelial glycocalyx: composition, functions, and visualization. Pflugers Archiv: European journal of physiology 454: 345–359. doi: 10.1007/s00424-007-0212-8 PMID: 17256154

15. VanTeeffelen JW, Brands J, Vink H (2010) Agonist-induced impairment of glycocalyx exclusion properties: contribution to coronary effects of adenosine. Cardiovascular research 87: 311–319. doi: 10.1093/cvr/cvq114 PMID: 20418474

16. Padberg JS, Wiesinger A, di Marco GS, Reuter S, Grabner A, et al. (2014) Damage of the endothelial glycocalyx in chronic kidney disease. Atherosclerosis 234: 335–343. doi: 10.1016/j.atherosclerosis.2014.03.016 PMID: 24727235

17. Cai B, Fan J, Zeng M, Zhang L, Fu BM (2012) Adhesion of malignant mammary tumor cells MDA-MB-231 to microvessel wall increases microvascular permeability via degradation of endothelial surface glycocalyx. J Appl Physiol (1985) 113: 1141–1153. doi: 10.1152/japplphysiol.00479.2012

18. Forstermann U, Sessa WC (2012) Nitric oxide synthases: regulation and function. European heart journal 33: 829–837, 837a–837d. doi: 10.1093/eurheartj/ehr304 PMID: 21890489

19. Cooke JP, Stamler J, Andon N, Davies PF, McKinley G, et al. (1990) Flow stimulates endothelial cells to release a nitrovasodilator that is potentiated by reduced thiol. Am J Physiol 259: H804–812. PMID: 2396689

20. Forstermann U, Munzel T (2006) Endothelial nitric oxide synthase in vascular disease: from marvel to menace. Circulation 113: 1708–1714. doi: 10.1161/CIRCULATIONAHA.105.602532 PMID: 16585403

21. Florian JA, Kosky JR, Ainslie K, Pang Z, Dull RO, et al. (2003) Heparan sulfate proteoglycan is a mechanosensor on endothelial cells. Circulation research 93: e136–142. doi: 10.1161/01.RES.0000101744.47866.D5 PMID: 14563712

22. Ziegler T, Bouzourene K, Harrison VJ, Brunner HR, Hayoz D (1998) Influence of oscillatory and unidirectional flow environments on the expression of endothelin and nitric oxide synthase in cultured endothelial cells. Arteriosclerosis, thrombosis, and vascular biology 18: 686–692. doi: 10.1161/01.ATV.18.5.686 PMID: 9598825

23. Pritchard KA Jr, Groszek L, Smalley DM, Sessa WC, Wu M, et al. (1995) Native low-density lipoprotein increases endothelial cell nitric oxide synthase generation of superoxide anion. Circulation research 77: 510–518. doi: 10.1161/01.RES.77.3.510 PMID: 7543827

24. Guo X, Kassab GS (2009) Role of shear stress on nitrite and NOS protein content in different size conduit arteries of swine. Acta Physiol (Oxf) 197: 99–106. doi: 10.1111/j.1748-1716.2009.01999.x

25. Pohl U, Herlan K, Huang A, Bassenge E (1991) EDRF-mediated shear-induced dilation opposes myogenic vasoconstriction in small rabbit arteries. Am J Physiol 261: H2016–2023. PMID: 1721502

26. Kuchan MJ, Frangos JA (1994) Role of calcium and calmodulin in flow-induced nitric oxide production in endothelial cells. Am J Physiol 266: C628–636. PMID: 8166225

27. Pahakis MY, Kosky JR, Dull RO, Tarbell JM (2007) The role of endothelial glycocalyx components in mechanotransduction of fluid shear stress. Biochem Biophys Res Commun 355: 228–233. doi: 10.1016/j.bbrc.2007.01.137 PMID: 17291452

28. Lopez-Quintero SV, Amaya R, Pahakis M, Tarbell JM (2009) The endothelial glycocalyx mediates shear-induced changes in hydraulic conductivity. American journal of physiology Heart and circulatory physiology 296: H1451–1456. doi: 10.1152/ajpheart.00894.2008 PMID: 19286951

29. Koo A, Nordsletten D, Umeton R, Yankama B, Ayyadurai S, et al. (2013) In silico modeling of shear-stress-induced nitric oxide production in endothelial cells through systems biology. Biophys J 104: 2295–2306. doi: 10.1016/j.bpj.2013.03.052 PMID: 23708369

30. Stevens HY MB, Bell KS, Yun S, Yeh JC, Frangos JA (2008) PECAM-1 is a critical mediator of atherosclerosis. Disease Models & Mechanisms 1: 175–181. doi: 10.1242/dmm.000547

31. Schwartz MA, DeSimone DW (2008) Cell adhesion receptors in mechanotransduction. Curr Opin Cell Biol 20: 551–556. doi: 10.1016/j.ceb.2008.05.005 PMID: 18583124

32. Gojova A, Barakat AI (2005) Vascular endothelial wound closure under shear stress: role of membrane fluidity and flow-sensitive ion channels. J Appl Physiol (1985) 98: 2355–2362. doi: 10.1152/japplphysiol.01136.2004

33. Gautam M, Shen Y, Thirkill TL, Douglas GC, Barakat AI (2006) Flow-activated chloride channels in vascular endothelium. Shear stress sensitivity, desensitization dynamics, and physiological implications. J Biol Chem 281: 36492–36500. doi: 10.1074/jbc.M605866200 PMID: 16973617

34. Yamamoto K, Ando J (2011) New molecular mechanisms for cardiovascular disease:blood flow sensing mechanism in vascular endothelial cells. J Pharmacol Sci 116: 323–331. doi: 10.1254/jphs.10R29FM PMID: 21757846

35. Tabouillot T, Muddana HS, Butler PJ (2011) Endothelial Cell Membrane Sensitivity to Shear Stress is Lipid Domain Dependent. Cell Mol Bioeng 4: 169–181. doi: 10.1007/s12195-010-0136-9 PMID: 22247740

36. Egorova AD vdHK, Poelmann RE, Hierck BP (2012) Primary cilia as biomechanical sensors in regulating endothelial function. Differentiation 83: S56–61. doi: 10.1016/j.diff.2011.11.007 PMID: 22169885

37. Matsui TS, Kaunas R, Kanzaki M, Sato M, Deguchi S (2011) Non-muscle myosin II induces disassembly of actin stress fibres independently of myosin light chain dephosphorylation. Interface Focus 1: 754–766. doi: 10.1098/rsfs.2011.0031 PMID: 23050080

38. Morgan JT, Pfeiffer ER, Thirkill TL, Kumar P, Peng G, et al. (2011) Nesprin-3 regulates endothelial cell morphology, perinuclear cytoskeletal architecture, and flow-induced polarization. Mol Biol Cell 22: 4324–4334. doi: 10.1091/mbc.E11-04-0287 PMID: 21937718

39. Wang N, Tytell JD, Ingber DE (2009) Mechanotransduction at a distance: mechanically coupling the extracellular matrix with the nucleus. Nat Rev Mol Cell Biol 10: 75–82. doi: 10.1038/nrm2594 PMID: 19197334

40. Kang H, Fan Y, Deng X (2011) Vascular smooth muscle cell glycocalyx modulates shear-induced prolif-eration, migration, and NO production responses. American journal of physiology Heart and circulatory physiology 300: H76–83. doi: 10.1152/ajpheart.00905.2010 PMID: 21037235

41. Juffer P, Bakker AD, Klein-Nulend J, Jaspers RT (2014) Mechanical loading by fluid shear stress of myotube glycocalyx stimulates growth factor expression and nitric oxide production. Cell Biochem Bio-phys 69: 411–419. doi: 10.1007/s12013-013-9812-4 PMID: 24402674

42. Mochizuki S, Vink H, Hiramatsu O, Kajita T, Shigeto F, et al. (2003) Role of hyaluronic acid glycosami-noglycans in shear-induced endothelium-derived nitric oxide release. American journal of physiology Heart and circulatory physiology 285: H722–726. PMID: 12730059

43. Kumagai R, Lu X, Kassab GS (2009) Role of glycocalyx in flow-induced production of nitric oxide and reactive oxygen species. Free Radic Biol Med 47: 600–607. doi: 10.1016/j.freeradbiomed.2009.05.034 PMID: 19500664

44. Giantsos-Adams KM, Koo AJ, Song S, Sakai J, Sankaran J, et al. (2013) Heparan Sulfate Regrowth Profiles Under Laminar Shear Flow Following Enzymatic Degradation. Cell Mol Bioeng 6: 160–174. doi: 10.1007/s12195-013-0273-z PMID: 23805169

45. Koo A, Dewey CF Jr, Garcia-Cardena G (2013) Hemodynamic shear stress characteristic of athero-sclerosis-resistant regions promotes glycocalyx formation in cultured endothelial cells. Am J Physiol Cell Physiol 304: C137–146. doi: 10.1152/ajpcell.00187.2012 PMID: 23114962

46. Zeng Y, Tarbell JM (2014) The adaptive remodeling of endothelial glycocalyx in response to fluid shear stress. PLoS One 9: e86249. doi: 10.1371/journal.pone.0086249 PMID: 24465988

47. Yao Y, Rabodzey A, Dewey CF Jr (2007) Glycocalyx modulates the motility and proliferative response of vascular endothelium to fluid shear stress. American journal of physiology Heart and circulatory physiology 293: H1023–1030. doi: 10.1152/ajpheart.00162.2007 PMID: 17468337

48. VanTeeffelen JW, Brands J, Jansen C, Spaan JA, Vink H (2007) Heparin impairs glycocalyx barrier properties and attenuates shear dependent vasodilation in mice. Hypertension 50: 261–267. doi: 10.1161/HYPERTENSIONAHA.107.089250 PMID: 17452501

49. Zhou X, He P (2011) Improved measurements of intracellular nitric oxide in intact microvessels using 4,5-diaminofluorescein diacetate. American journal of physiology Heart and circulatory physiology 301: H108–114. doi: 10.1152/ajpheart.00195.2011 PMID: 21536843

50. Yen WY, Cai B, Zeng M, Tarbell JM, Fu BM (2012) Quantification of the endothelial surface glycocalyx on rat and mouse blood vessels. Microvascular research. doi: 10.1016/j.mvr.2012.02.005 PMID: 22349291

51. Fu BM, Shen S (2004) Acute VEGF effect on solute permeability of mammalian microvessels in vivo. Microvascular research 68: 51–62. doi: 10.1016/j.mvr.2004.03.004 PMID: 15219420

52. Shen S, Fan J, Cai B, Lv Y, Zeng M, et al. (2010) Vascular endothelial growth factor enhances cancer cell adhesion to microvascular endothelium in vivo. Experimental physiology 95: 369–379. doi: 10.1113/expphysiol.2009.050260 PMID: 19880535

53. Chappell D, Jacob M, Rehm M, Stoeckelhuber M, Welsch U, et al. (2008) Heparinase selectively sheds heparan sulphate from the endothelial glycocalyx. Biol Chem 389: 79–82. doi: 10.1515/BC.2008.005 PMID: 18095872

54. Guo P, Cai B, Lei M, Liu Y, Fu BM (2014) Differential arrest and adhesion of tumor cells and microbeads in the microvasculature. Biomech Model Mechanobiol 13: 537–550. doi: 10.1007/s10237-013-0515-y PMID: 23880911

55. Liu Q, Mirc D, Fu BM (2008) Mechanical mechanisms of thrombosis in intact bent microvessels of rat mesentery. J Biomech 41: 2726–2734. doi: 10.1016/j.jbiomech.2008.06.013 PMID: 18656200

56. Baker M, Wayland H (1974) On-line volume flow rate and velocity profile measurement for blood in microvessels. Microvascular research 7: 131–143. doi: 10.1016/0026-2862(74)90043-0 PMID: 4821168

57. Williams DA (2007) Change in shear stress (Deltatau)/hydraulic conductivity (Lp) relationship after pro-nase treatment of individual capillaries in situ. Microvascular research 73: 48–57. doi: 10.1016/j.mvr.2006.08.003 PMID: 17030043

58. Kojima H NN, Kikuchi K, Urano Y, Higuchi T, Tanaka J, et al. (1998) Direct evidence of NO production in rat hippocampus and cortex using a new fluorescent indicator: DAF-2 DA. NeuroReport 9: 3345–3348. doi: 10.1097/00001756-199810260-00001 PMID: 9855277

59. Yi FX, Zhang AY, Campbell WB, Zou AP, Van Breemen C, et al. (2002) Simultaneous in situ monitoring of intracellular Ca2+ and NO in endothelium of coronary arteries. American journal of physiology Heart and circulatory physiology 283: H2725–2732. PMID: 12388315

60. Zhu L, He P (2005) Platelet-activating factor increases endothelial [Ca2+]i and NO production in individually perfused intact microvessels. American journal of physiology Heart and circulatory physiology 288: H2869–2877. doi: 10.1152/ajpheart.01080.2004 PMID: 15665052

61. Reitsma S, oude Egbrink MG, Vink H, van den Berg BM, Passos VL, et al. (2011) Endothelial glycocalyx structure in the intact carotid artery: a two-photon laser scanning microscopy study. J Vasc Res 48: 297–306. doi: 10.1159/000322176 PMID: 21273784

62. Chang YS, Yaccino JA, Lakshminarayanan S, Frangos JA, Tarbell JM (2000) Shear-induced increase in hydraulic conductivity in endothelial cells is mediated by a nitric oxide-dependent mechanism. Arteriosclerosis, thrombosis, and vascular biology 20: 35–42. doi: 10.1161/01.ATV.20.1.35 PMID: 10634798

63. Rosenberg RD, Shworak NW, Liu J, Schwartz JJ, Zhang L (1997) Heparan sulfate proteoglycans of the cardiovascular system. Specific structures emerge but how is synthesis regulated? J Clin Invest 100: S67–75.

64. Ebong EE, Lopez-Quintero SV, Rizzo V, Spray DC, Tarbell JM (2014) Shear-induced endothelial NOS activation and remodeling via heparan sulfate, glypican-1, and syndecan-1. Integr Biol (Camb) 6: 338–347. doi: 10.1039/c3ib40199e

65. Gao L, Lipowsky HH (2010) Composition of the endothelial glycocalyx and its relation to its thickness and diffusion of small solutes. Microvascular research 80: 394–401. doi: 10.1016/j.mvr.2010.06.005 PMID: 20600162

66. Zeng Y, Ebong EE, Fu BM, Tarbell JM (2012) The structural stability of the endothelial glycocalyx after enzymatic removal of glycosaminoglycans. PLoS One 7: e43168. doi: 10.1371/journal.pone.0043168 PMID: 22905223

67. Tarbell JM (2010) Shear stress and the endothelial transport barrier. Cardiovascular research 87: 320–330. doi: 10.1093/cvr/cvq146 PMID: 20543206